CIENCIA 9(2), 139-154, 2001
Maracaibo, Venezuela

Environmental catalysis and the chemistry of SO_2 on oxide surfaces: fundamental principles for the cleavage of S-O bonds

José A. Rodríguez
Department of Chemistry, Brookhaven National Laboratory. Upton, NY 11973, USA.
Fax: 1-631-344-5815. E-mail: rodrigez@bnl.gov

Recibido: 28-05-01 Aceptado: 12-06-01

Abstract

The rational design of catalysts with a high efficiency for the destruction of SO_2 (DeSOx process) is a major problem in environmental chemistry. This article presents an overview of recent studies that use synchrotron-based photoemission, x-ray near edge absorption spectroscopy, and first-principles density functional calculations to examine the interaction of SO_2 with single-crystal surfaces and powders of oxides. On pure stoichiometric oxides (MgO, Al_2O_3, TiO_2, Cr_2O_3, Fe_2O_3, NiO, CuO, ZnO, ZrO_2, V_2O_5, MoO_3, $CoMoO_4$ and $NiMoO_4$), SO_2 reacts with the O centers to form SO_3 or SO_4 species that decompose at elevated temperatures. Adsorption on the metal cations occurs below 300 K and does not lead to cleavage of S-O bonds. In typical oxides, the occupied cation bands are too stable for effective bonding interactions with the LUMO of SO_2. *To activate an oxide for S-O bond cleavage, one has to generate occupied metal states above the valence band of the oxide.* This basic requirement can be accomplished by the creation of O vacancies, alkali (Na, K, Cs) promotion, or doping with a transition metal. Metal dopants are useful for inducing the formation of O vacancies in many oxides. In addition, a dopant agent can directly introduce occupied states within the band gap of an oxide. For $TM_xMg_{1-x}O$ systems (TM= Zn, Sn, Ni, Co, Fe, Mn, or Cr), a correlation is found between the energy position of the dopant-induced states and the ability of the mixed-metal oxide to break S-O bonds. The behavior of the $Cr_xMg_{1-x}O$ system illustrates a fundamental principle for the design of DeSOx catalyst.

Keywords: DeSOx; environmental catalysis; metal oxides; sulfur dioxide.

Catálisis ambiental y la química de SO_2 sobre superficies de óxidos: principios fundamentales de la ruptura de los enlaces S-O

Resumen

El diseño de catalizadores con una alta actividad para la destrucción de SO_2 (procesos DeSOx) es uno de los objetivos prioritarios en la catálisis ambiental. Este artículo presenta una revisión de trabajos recientes donde se estudia la adsorción y química de SO_2 sobre óxidos utilizando espectroscopías de fotoemisión y absorción de rayos x, y cálculos basados en la teoría del

funcional de la densidad electrónica. Sobre óxidos puros estequiometricos (MgO, Al_2O_3, TiO_2, Cr_2O_3, Fe_2O_3, NiO, CuO, ZnO, ZrO_2, V_2O_5, MoO_3, $CoMoO_4$ and $NiMoO_4$), SO_2 reacciona con los átomos de O formando grupos SO_3 y SO_4 que descomponen a temperaturas elevadas. Adsorción sobre los cationes ocurre a temperaturas por debajo de los 300 K sin ruptura de enlaces S-O. En óxidos tipicos, las bandas de valencia de los cationes son demasiado estables como para interaccionar con el LUMO de SO_2. *Para romper enlaces S-O sobre un óxido, se necesita crear estados ocupados sobre las bandas de valencia que tengan carácter metálico.* Este requisito básico se puede obtener creando vacancias de O, depositando metales alcalinos sobre el óxido, o mediante el dopaje con metales de transición.

Palabras clave: Catálisis ambiental; DeSOx; dióxido de azufre; óxidos de metales.

1. Introduction

The chemistry of sulfur dioxide (SO_2) on oxide surfaces is receiving a lot of attention due to its importance in the industrial production of sulfuric acid (1) and environmental catalysis (2- 4). Sulfur-containing molecules are common impurities present in coal and crude oil. SO_2 is one of the major air pollutants released to the atmosphere as a result of the combustion of fuels in power plants, factories, houses and transportation. It contributes to the generation of smog and constitutes a serious health hazard for the respiratory system After its oxidation and reaction with water in the atmosphere, it is responsible for the acid rain that kills vegetation and corrodes buildings and monuments in modern cities (2). In addition, the SO_2 produced by the combustion of sulfur-containing fuels in automotive engines poisons the catalysts that are used for the removal of CO and NO in exhaust catalytic converters ($2CO + O_2 \rightarrow 2CO_2$; $2CO + 2NO \rightarrow 2CO_2 + N_2$) (4,5). When SO_2 is present in the catalytic converter at high concentrations, it dissociates on the precious-metal component of the catalyst (Rh, Pd or Pd), blocking active sites and reducing also the overall activity of the system through medium or long-range electronic effects (6,7). At the levels of 5 to 20 ppm currently present in the typical automotive exhaust, SO_2 interacts primarily with the ceria component of the catalytic converter, and the poisoning of this oxide is a major concern nowadays (8-10).

Governments are constantly tightening regulations to limit the production of SO_2 and emission of sulfur compounds into the air (3-5). Over the past 30 years several processes have been proposed and developed for the removal of SO_2 from exhaust systems, DeSOx operations, (3-5,11). There is still not universally acceptable solution to this problem. Due to their low cost, oxides are frequently used as sorbents or scrubbers for trapping the SO_2 molecule in industrial processes (11). There is a general interest (3,4,11-15) in using oxides as catalysts for the Claus reaction ($SO_2 + 2H_2S \rightarrow 2H_2O + 3S_n$) and the reduction of sulfur dioxide by CO ($SO_2 + 2CO \rightarrow 2CO_2 + S_n$). In these reactions, the rupture of the S-O bonds on the oxide catalyst is one of the most difficult steps. For a rational design of efficient DeSOx catalysts, one needs a fundamental understanding of the chemistry of SO_2 on oxides.

This article presents an overview of recent studies that use synchrotron-based photoemission, x-ray near edge absorption spectroscopy (XANES), and first-principles density functional calculations to examine the interaction of SO_2 with well-defined surfaces and powders of oxides. The use of single crystals like ZnO(0001), MgO(100) or TiO_2(110) allows a detailed comparison of the chemical activity of oxygen and metal centers in oxides, plus the study of struc-

ture sensitivity and the effects of defects and O vacancies. This review article is organized as follows. First, a general description of the behavior of SO_2 on pure stoichiometric oxide systems is presented. This is followed by an analysis of the problems associated with the cleavage of S-O bonds on oxides. Finally, three different approaches for facilitating or promoting the dissociation of SO_2 are discussed.

2. Chemistry of SO_2 on pure oxides

Zinc oxide is frequently used in the chemical and petrochemical industries as a sorbent to trap sulfur-containing molecules. The adsorption of SO_2 was investigated on ZnO(000$\bar{1}$)-O, ZnO(0001)-Zn and polycrystalline ZnO powders (16, 17). Figure 1 shows S 2p photoemission spectra acquired after dosing SO_2 to the O terminated face of zinc oxide, ZnO(000$\bar{1}$)-O. A well-defined doublet is seen with the $2p_{3/2}$ component at ~ 166.4 eV. This indicates the presence of SO_3 formed by reaction of SO_2 with the O centers of the oxide (16):

$$SO_2(gas) + O(surf) \rightarrow SO_3(ads) \quad [1]$$

After an SO_2 dose of 2 langmuir (L), features for physisorbed SO_2 appear between 168 and 171 eV (16, 17). The physisorbed molecules desorb upon heating to 150 K, and only 0.4 monolayers (ML) of SO_3 remain on the oxide substrate. The adsorbed SO_3 was stable up to ~ 400 K, where it began to decompose with SO_2 desorbing into gas phase (16). Thus, relatively strong interactions occur between SO_2 and the O terminated ZnO(000$\bar{1}$) surface. In contrast, weak bonding was observed between SO_2 and the Zn terminated face of zinc oxide, ZnO(0001)-Zn (17). On this system, SO_2 was adsorbed at 100 K, but upon heating to 200 K all the Zn-SO_2 bonds were broken without dissociation of the adsorbate.

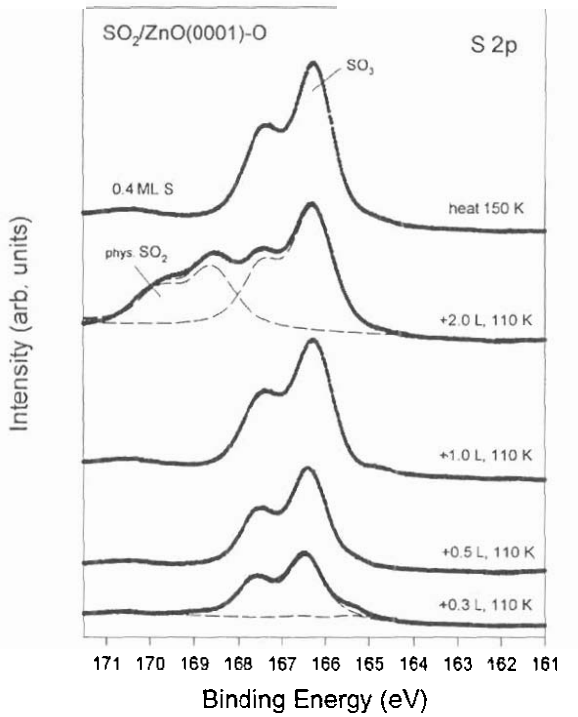

Figure 1. S 2p photoemission spectra for the adsorption of SO_2 on the O-terminated face of ZnO. (16). The dosing of SO_2 (0.3, 0.5, 1.0, and 2.0 langmuir) was performed at 110 K and in the final step the sample was annealed to 150 K.

Figure 2 shows XANES spectra at the S K-edge for a ZnO powder exposed to 500 Torr of SO_2 at 323 K. For this and smaller doses (5, 10, 50 Torr) of sulfur dioxide, there was only one clear peak in the spectrum with the maximum at a photon energy of ~ 2478 eV. Such a peak position denotes the formation of SO_3 (16). Upon heating from 323 to 373 K, the intensity of the signal for SO_3 decreases and a weak feature appears between 2481 and 2483 eV that could be attributed to a small amount of SO_4 (16). This weak feature is still visible after heating to 623 K. On the rough polycrystalline surface of ZnO, there was a lack of strong Zn-SO_2 bonding interactions and no S-O bond

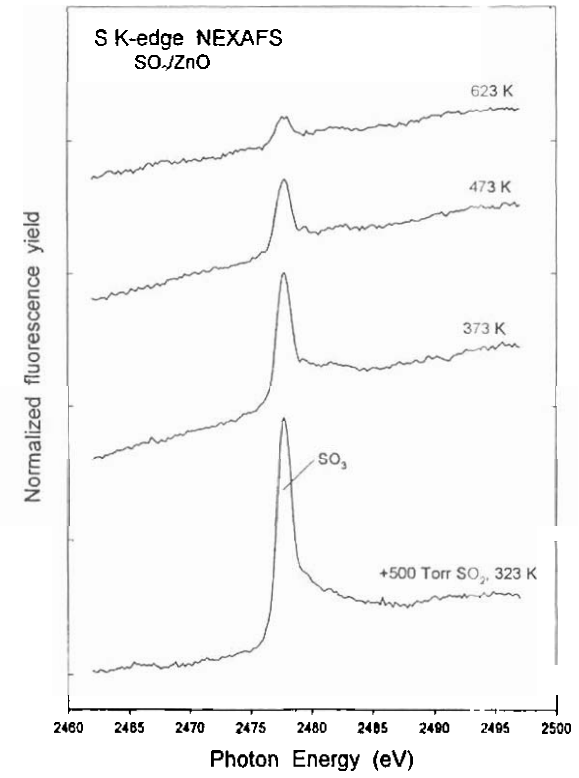

Figure 2 X-ray absorption spectra (S K-edge) for the adsorption of SO_2 on a polycrystalline powder of zinc oxide (16). The sample was exposed to 500 Torr of SO_2 at 323 K and, after evacuation of the gas, annealed in vacuum to the indicated temperatures.

cleavage as was observed on the ZnO(0001)-Zn single crystal (17).

As zinc oxide, magnesium oxide can be used as a sorbent to remove SO_2 in industrial applications (11). Figure 3 displays photoemission data for the adsorption of SO_2 at 300 K on a MgO(100) crystal, bottom panel, and a MgO(100) epitaxial film grown on a Mo(100) substrate, top panel (18). The (100) face of MgO consist of a 50%-50% mixture of Mg and O atoms. The photoemission data indicate that only the O atoms interact strongly with SO_2 forming a mixture of SO_3 and SO_4 species on the oxide surface (18). An identical result was observed with XANES after exposing MgO powders to moderate pressures of SO_2 (19). The metal centers of MgO interact weakly with SO_2 and are not able to dissociate the molecule (18-21). In general, bulk powders of pure stoichiometric oxides (MgO, Al_2O_3, TiO_2, Cr_2O_3, Fe_2O_3, NiO, CuO, ZnO, ZrO_2, V_2O_5, MoO_3, $CoMoO_4$ and $NiMoO_4$) do not decompose SO_2 (12, 13, 16-25). Well-defined surfaces of oxides that expose metal cations with a high coordination number (MgO(100), ZnO(0001), TiO_2(110), NiO(001), V_2O_5(0001), Fe_2O_3(0001)) also do not dissociate SO_2 (17, 18, 26-30). Thus, stoichiometric oxides can be very good as sorbents

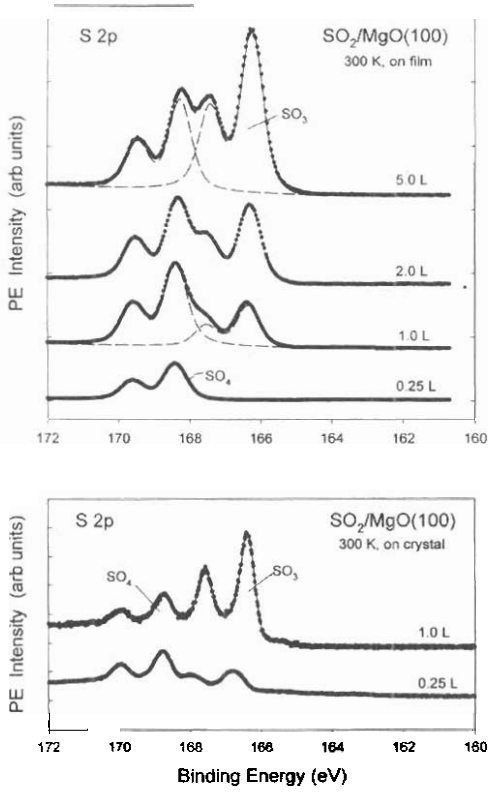

Figure 3. S 2p photoemission spectra for the adsorption of SO_2 on a MgO(100) single crystal and a MgO(100) epitaxial film grown on a Mo(100) substrate, . (18).

(forming SO_3 or SO_4 species), but in general they will not be active as catalysts for reactions that involve S-O bond cleavage.

At a theoretical level, the bonding between SO_2 and the cations of oxides has been investigated using cluster models (MgO, CaO, ZnO, MoO_2 (20, 31-33)) or extended two-dimensional slabs (MgO (19, 21)). In all the theoretical calculations, the frontier molecular orbitals of SO_2 mix poorly with electronic states located on the metal centers of the oxides. Figure 4 compares the band energies of two typical oxides (Al_2O_3 and ZnO) and the molecular orbital energies of SO_2 (34, 35). For the oxides, the empty and occupied bands are indicated by dotted and solid lines, respectively. The lowest unoccupied molecular orbital (LUMO) of SO_2 is S-O antibonding (32, 34). In typical oxides, the occupied states of the metal centers are *too stable* for interacting or transferring electron density into the LUMO of SO_2 (i.e. no effective band-orbital mixing). This leads to small SO_2 adsorption energies on the cations and prevents dissociation of the molecule (19, 20, 31). *To dissociate SO_2 on an oxide surface, one needs to create occupied metal states above the valence band of the oxide.* In the following sections, we will discuss three different approaches to accomplish this.

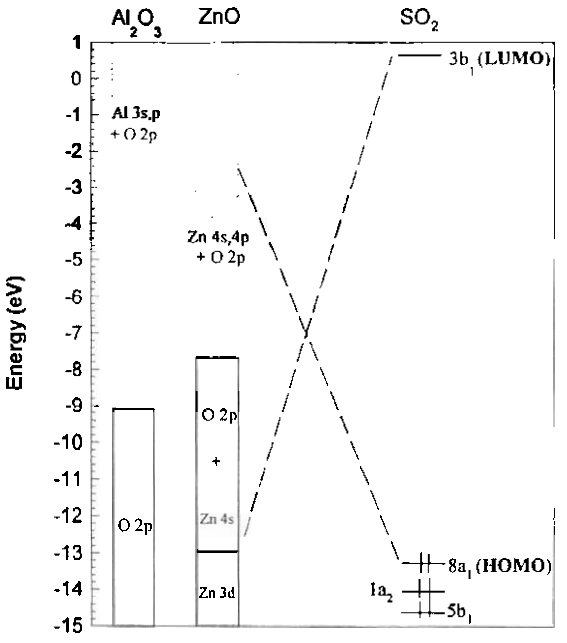

Figure 4. Energy position for the valence and conduction bands of Al_2O_3 and ZnO. Empty states are shown as doted lines, while solid lines denote occupied states. For comparison, we also include the molecular orbital energies of SO_2. The zero of energy is the vacuum level (34, 35).

3. O vacancies in oxides and SO_2 dissociation

A study of the interaction of SO_2 with CeO_2 is interesting for two basic reasons. First, ceria doped with copper or other metals is able to catalyze the reduction of SO_2 by CO (14, 15). And second, adsorption of SO_2 affects the performance of ceria in automotive catalytic converters (8-10). The right-side panel in Figure 5 shows S 2p photoemission results for the adsorption of SO_2 on several ceria systems (23). The left-panel displays the corresponding valence photoemission spectra for the ceria systems *before* the adsorption of SO_2 (23). In the case of CeO_2, the valence spectrum shows no signal in the region between 4 and 0 eV, where Ce^{3+} appears (36). The features between 8 and 4 eV contain O 2p character (main component) *and* metal character (37). On this system, the adsorption of SO_2 mainly produces SO_4 (23). O atoms can be preferentially removed from CeO_2 by Ar^+ sputtering (36). In Figure 5, the valence spectra for CeO_{2-x} and Ce_2O_{3+x} are characterized by a Ce^{3+} peak near 2 eV (23). Thus, the introduction of O vacancies creates occupied metal states above the valence band of CeO_2. This, phenomenon should make the oxide active for the dissociation S-O bonds (see above). And, indeed, the S 2p data exhibit features between 164 and 162 eV that come from the

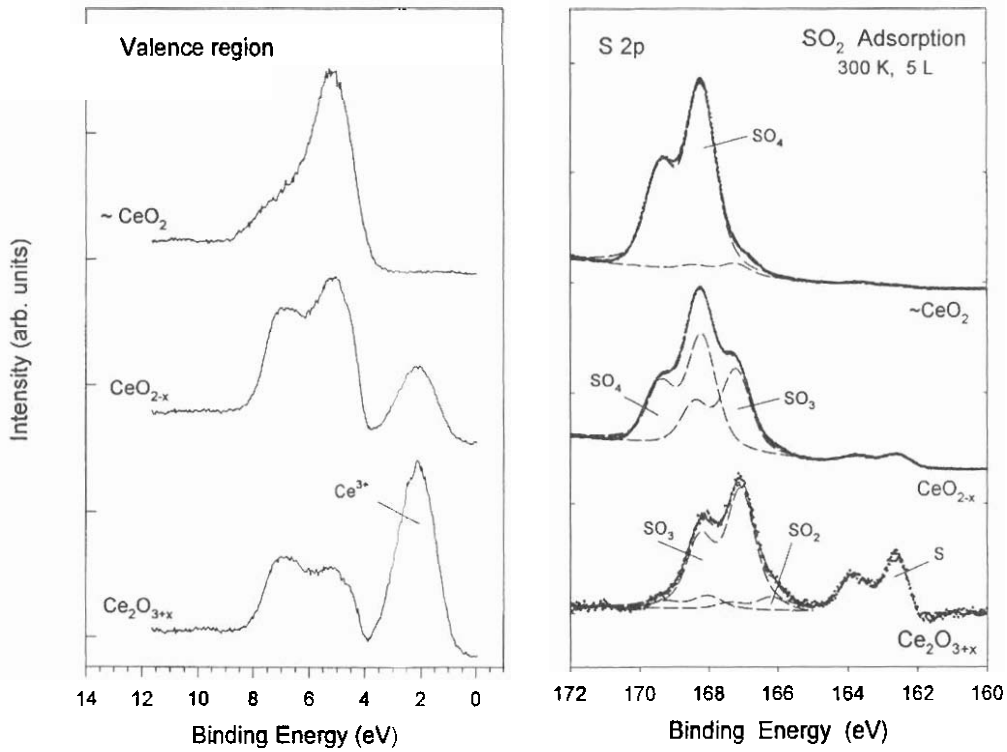

Figure 5. Right-side: Valence photoemission spectra for a series of ceria systems. Left- side: S 2p spectra taken after dosing 5 langmuir of SO_2 at 300 K to the ceria surfaces (23).

full decomposition of the SO_2 molecule on CeO_{2-x} and Ce_2O_{3+x}. CeO_2 is useful as a catalysts for the reduction of SO_2 by CO only at elevated temperatures, when CO is able to create O vacancies and associated Ce^{3+} sites in the oxide (23, 38).

Figure 6 shows S 2p spectra taken after exposing a MgO_{1-x}(100) surface to SO_2 at 300 K (19). O vacancies and defects were created by briefly sputtering a MgO(100) surface with Ar^+ ions at 300 K. This led to a broadening of the Mg 2p core level towards the low binding-energy side (i.e. net reduction in the average oxidation state of Mg) and produced new occupied states above the valence band of stoichiometric MgO (39). The S2p data in Figure 6 point out the coexistence of S, SO_3 and SO_4 on the oxide substrate upon adsorption of SO_2. A comparison of the results in Figure 3 and 6 indicates

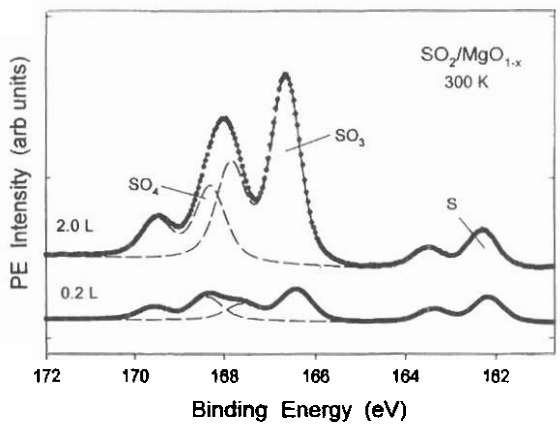

Figure 6. S 2p photoemission data for the adsorption of SO_2 on a MgO_{1-x}(100) surface (19). 0.2 and 2.0 L were dosed to the oxide surface at 300K.

that O vacancies facilitate the dissociation of SO_2 on MgO(100). Theoretical calculations show that on these defects the adsorption energy of SO_2 is much larger than on a flat MgO(100) surface with a substantial weakening and elongation of the S-O bonds (20,21,24). TiO_2(110), NiO(001), V_2O_5(0001) and Fe_2O_3(0001) also become active for the decomposition of SO_2 after the creation of O vacancies by ion sputtering (26-30).

In principle, oxides that can be reduced by CO to form O vacancies, could be active catalysts for the $2CO_{gas} + SO_{2,gas} \rightarrow 2CO_{2,gas} + S_{ads}$ reaction. This is the case of CuO and CeO_2 (14,15,23,38). To favor the formation of O vacancies and active centers in these oxide, the reaction is usually carried out at high temperatures with a CO/SO_2 ratio in the feed ≥ 2. In the case of ceria, doping with a second metal helps the formation of O vacancies (37, 40) and increases catalytic activity (14, 15, 38, 40).

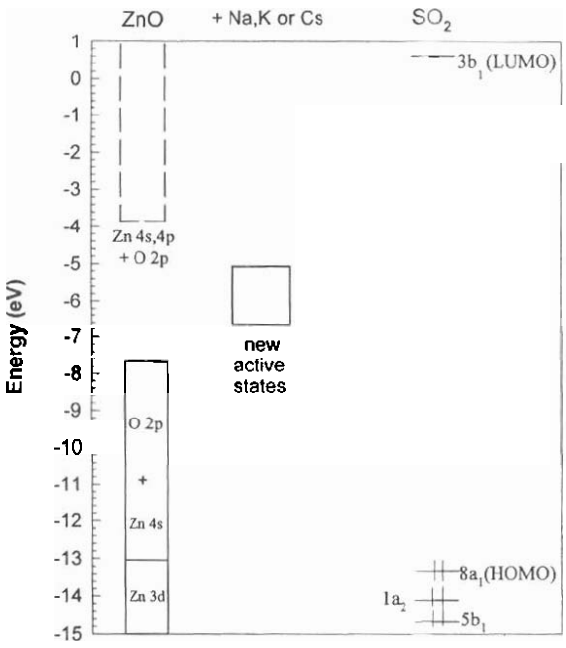

Figure 7. Energy positions for the bands of ZnO, the molecular orbitals of SO_2 and occupied states generated by the deposition of alkali metals on the oxide (34, 45, 46). For ZnO, empty states are shown as doted lines, while solid lines denote occupied states. The zero of energy is the vacuum level.

4. Alkali promotion of oxides and SO_2 dissociation

It is well-established that the activity of an oxide catalyst or sorbent in the DeSOx process can be enhanced by the addition of an alkali metal (41-43). In general, the DeSOx catalysts or sorbents are complex systems and the exact role of the alkali in the removal process is poorly understood. The electronic interactions between an alkali metal and an oxide can range from very strong to weak (44), opening the possibility for large variations in chemical reactivity. Figure 7 shows the energy positions for the bands of pure ZnO and occupied states generated after depositing alkali metals (Na, K, Cs) on the O or Zn terminated faces of this oxide (24, 34, 45, 46). Potassium and cesium bond very strongly to the ZnO(000$\bar{1}$)-O surface forming $(\sqrt{3}x\sqrt{3})$ superstructures (47,48). The bonding to the ZnO(0001)-Zn surface is weaker (47,48), but on both surfaces the alkali metals behave as electron donors creating occupied states above the valence band of ZnO (24, 34, 45, 46). These extra states are close in energy to the LUMO of SO_2 (see Figure 7) and, therefore, are useful for promoting the dissociation of the molecule.

The adsorption of SO_2 on the $(\sqrt{3}x\sqrt{3})$-K/ZnO(000$\bar{1}$)-O and $(\sqrt{3}x\sqrt{3})$-Cs/ZnO(000$\bar{1}$)-O surfaces was investigated using photoemission (16). In Figure 8, a comparison of the data for pure ZnO(00$\bar{1}$)-O and the alkali-promoted surfaces (top panel) shows that potassium and cesium facilitate the full decomposition of SO_2 and deposition of sulfur on the surface. In this respect, potassium is somewhat better than cesium as a promoter. The dissociation of SO_2 accumulates extra oxygen on the surface that is

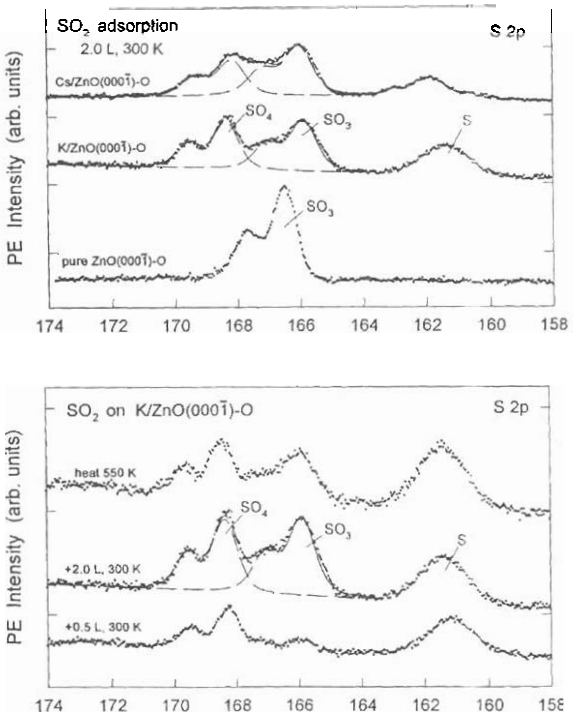

Figure 8. Top panel: S 2p spectra acquired after dosing 2 langmuir of sulfur dioxide to ZnO(000$\bar{1}$)-O,($\sqrt{3}$x$\sqrt{3}$)-K/ ZnO(000$\bar{1}$)-O, and ($\sqrt{3}$ x $\sqrt{3}$)-Cs/ ZnO(000$\bar{1}$)-O at 300 K. Bottom panel: S 2p spectra for the adsorption of SO_2 on the ($\sqrt{3}$ x $\sqrt{3}$)-K/ ZnO(000$\bar{1}$)-O surface. In the first step, 0.5 and 2.0 langmuir of SO_2 were dosed to the alkali-metal promoted surface at 300 K. This was followed by annealing to 550 K. (16).

used in the formation of SO_4. The S 2p spectra after an SO_2 dose of 2.0 langmuir show the coexistence of S, SO_3 and SO_4 on the {$\sqrt{3}$x$\sqrt{3}$}-K/ZnO(000$\bar{1}$)-O and {$\sqrt{3}$x$\sqrt{3}$}-Cs/ZnO(000$\bar{1}$)-O surfaces, whereas only SO_3 is seen on ZnO(000$\bar{1}$)-O.

The bottom panel in Figure 8 displays S 2p spectra taken after dosing 0.5 and 2.0 langmuir of SO_2 to {$\sqrt{3}$x$\sqrt{3}$} -K/ZnO(000$\bar{1}$)-O at 300 K with subsequent annealing to 550 K. The corresponding results for {$\sqrt{3}$x$\sqrt{3}$}-Cs/ZnO(000$\bar{1}$)-O exhibited similar trends and are not shown. After a small SO_2 dose of 0.5 langmuir, the dominant sulfur species on the surface is S, followed by SO_4, and a very minor amount of SO_3. At this stage most of the adsorbed SO_2 molecules dissociated on sites of the {$\sqrt{3}$x$\sqrt{3}$}-K/ZnO(000$\bar{1}$)-O surface that were very reactive. Once these adsorption sites became saturated with sulfur and oxygen, the formation of stable SO_x groups on the surface was possible. SO_3 and SO_4 were abundant on the surface upon a total dose of 2.0 langmuir of SO_2. Heating to 550 K led to decomposition of a fraction of the adsorbed SO_4/SO_3 with deposition of sulfur on the oxide and evolution of SO_2 into gas phase. Under similar conditions, only SO_3 was found on the pure ZnO(000$\bar{1}$)-O surface.

Cesium adatoms ($Cs^{\delta+}$) substantially increase the rate of adsorption of SO_2 (34), S_2 (45), H_2S (45) and thiophene (46) on polycrystalline zinc oxide. Thus, in general, doping with Cs is a good route for enhancing the performance of ZnO as a sorbent for sulfur-containing molecules (34,46). Positive effects are also observed after adding alkali atoms to MgO (18). In contrast to the case of alkali atoms on ZnO, Na atoms bonded to MgO(100) have a charge almost equal to zero (49). Figure 9 shows the calculated density-of-states for the occupied bands of MgO(100) and Na/MgO(100). The valence band in MgO(100) contains mainly O 2p character plus some Mg 3s character. After adding sodium to the oxide surface, occupied states with Na 3s character appear ~ 2.5 eV above the {O 2p + Mg 3s} band. These states are quite important for bonding interactions with the LUMO of SO_2. Density-functional slab calculations (18) predict SO_2 bonding energies on adsorption sites of Na/MgO(100) that are 30-40 kcal/mol larger than those on MgO(100). On pure MgO(100), the structural perturbations in the adsorbed SO_2 molecule are minimal with elongations of less than 0.05 Å in the S-O bonds (18, 20, 21). In the case of the {Na

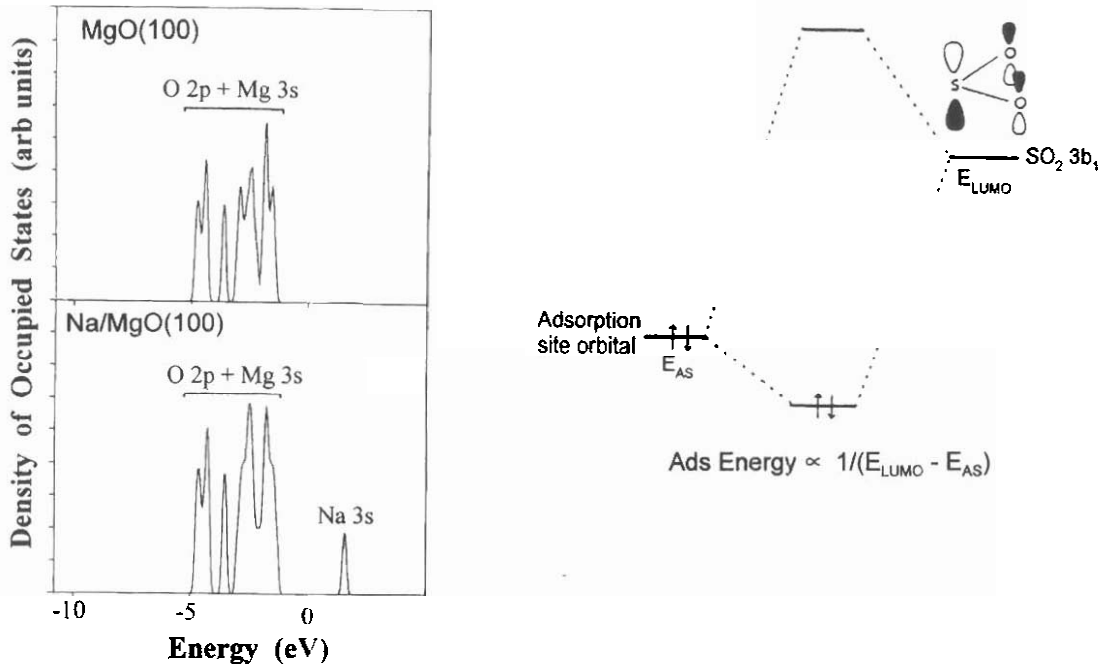

Figure . Left: calculated DOS for the occupied bands of MgO(100) and Na/MgO(100). The zero of energy is not the vacuum level (18). Right: Orbital interactions for the bonding of SO_2 to a metal center. According to perturbation theory (18,45,46): the smaller the energy separation between the interacting levels (E_{LUMO}-E_{AS}), the bigger the adsorption energy of SO_2.

+ SO_2]/MgO(100) system, there are elongations of 0.12-0.15 Å in the S-O bonds (18). For this system, Na donates charge (0.3-0.7 e) into the SO_2 LUMO weakening the S-O bonds. Eventually, this facilitates the dissociation of the SO_2 molecule (18).

Figure 10 displays typical S 2p spectra for the adsorption of SO_2 at 300 K on a MgO(100) single crystal and a MgO(100)/Mo(100) system both promoted with sodium. The spectra are complex and after a deconvolution (18) clear features are found for S, SO_2, SO_3 and SO_4. This can be contrasted to the results for the Na free surfaces (Figure 3) where only SO_3 and SO_4 were observed upon exposure to SO_2 at room temperature. At small exposures of SO_2 (<0.3 langmuir) the molecule completely dissociated on the Na/MgO(100) systems, yielding clear features for atomic sulfur in the S 2p region (18). Since no dissociation of SO_2 was seen on the clean oxide surfaces, one can conclude that the SO_2 molecules dissociated on the supported Na atoms or on sites near the Na-MgO interface. Subsequent doses of SO_2 gave S 2p features for chemisorbed SO_2 (163-165.5 eV) and the characteristic strong peaks for SO_3 and SO_4.

TiO_2 is frequently used as a sorbent/catalyst for the Claus reaction: $SO_2 + 2H_2S \rightarrow 2H_2O + S_{solid}$ (3). In the case of the Na/MgO(100) system discussed above, the alkali→oxide charge transfer is minimal and the occupied states produced above the oxide valence band are of Na character (18). The other extreme is represented by the cases of Na/TiO_2(110) and K/TiO_2(110), where there is a substantial alkali→oxide charge transfer (44, 50). This charge trans-

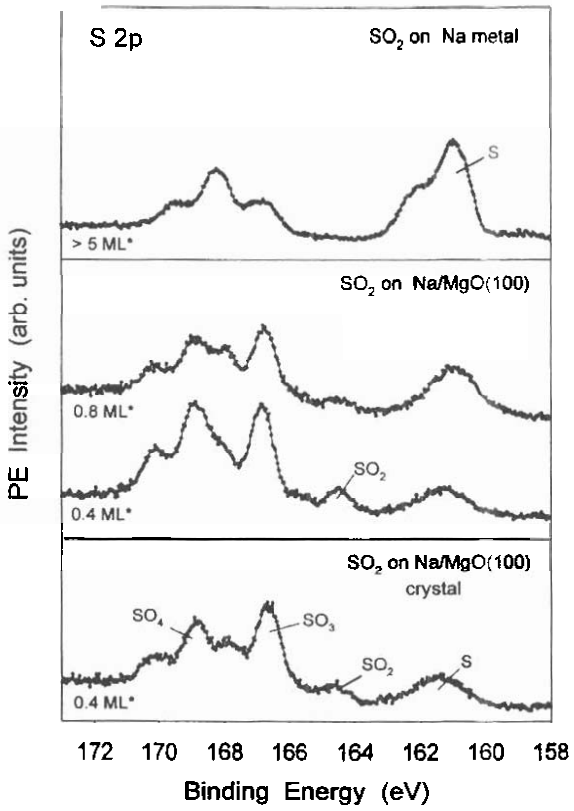

Figure 10. S 2p photoemission spectra for the adsorption of SO_2 on pure metallic sodium and Na/MgO(100) surfaces with sodium coverages of 0.4 and 0.8 equivalent monolayers. Before acquiring the spectra, 5 langmuir of SO_2 were dosed at 300 K (18).

fer reduces the density of occupied states of the alkali adatoms, but occupied states with Ti 3d character appear above the TiO_2 valence band (50). Energetically these new Ti 3d states are better positioned for interactions with the LUMO of SO_2 than normal states in the TiO_2 valence band. Recent photoemission experiments show full dissociation of SO_2 upon its adsorption on $K/TiO_2(110)$ surfaces at 300 K (24), whereas only SO_3/SO_4 is observed on a pure $TiO_2(110)$ substrate (26, 27).

5. Metal doping of oxides and SO_2 dissociation

Oxides that contain two metals can exhibit a higher activity for DeSOx processes than their single metal counterparts (14, 38, 40, 51). Recently, much attention has been focused on the performance of mixed-metal oxides in several areas of catalysis (15, 40, 52-54). In principle, the combination of two metals in an oxide matrix can produce materials with novel structural or electronic properties that can lead to superior catalytic activity or selectivity. In simple terms, the two metal centers can work in a cooperative way catalyzing different steps of a chemical process, or they can have an enhanced chemical activity due to the effects of metal–metal or metal–oxygen–metal interactions (40, 54). When dealing with the design of mixed-metal oxide catalysts for DeSOx reactions, it is important to know how to choose the "right" combination of metals. This can be a very complex issue (40, 54).

Metal dopants are useful for inducing the formation of O vacancies in many oxides (40, 55). For example, cation dopants with oxidation states lower than 4+ can be incorporated in the lattice of CeO_2 to produce O vacancies and Ce^{3+} sites active for the destruction of SO_2 (14, 37, 38, 40). Thus, the light-off temperature for the reduction of SO_2 by CO was lowered by 70 K after doping CeO_2 with 10% calcium (40). Several metal oxides are expected to be useful candidates as host matrixes for oxygen vacancy engineering through metal doping, e.g. oxides of Bi, Mo, Nb, Pr, Ti, V, W and Zr (40). In some cases, a metal dopant can favor O vacancy formation by inducing structural perturbations in the lattice of the oxide. For the doping of CeO_2 with Zr, the introduction of Zr induces shortening of the unit cell parameters (37) since the radius of Ce^{4+} (0.97 Å) is larger than that of Zr^{4+} (0.84 Å). The smaller size of the Zr^{4+} cations favors the formation of O vacancies by eliminating the strain associated with the transformation from Ce^{4+} to Ce^{3+} (56).

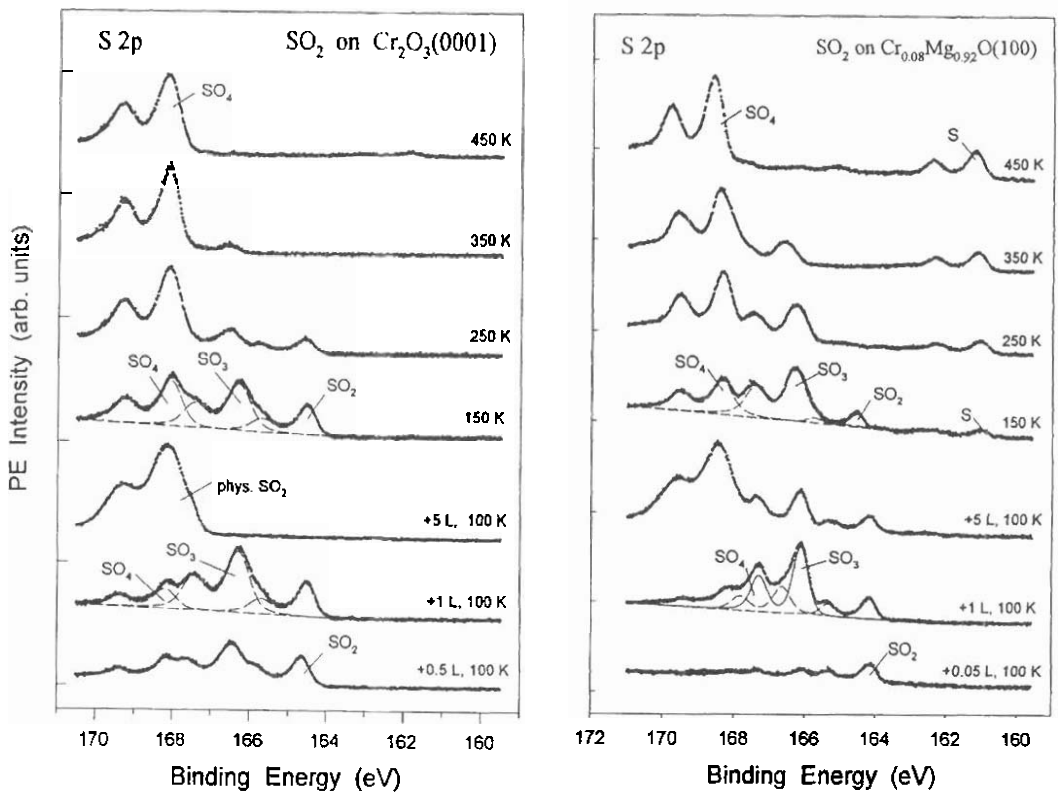

Figure 11. S 2p spectra for the adsorption of SO_2 on $Cr_2O_3(0001)$ and $Cr_{0.08}Mg_{0.92}O(100)$ surfaces at 100 K and subsequent heating to higher temperature. (51).

In addition to inducing O vacancies, a dopant agent can introduce occupied electronic states within the band gap of an oxide. This type of electronic states are particularly important for the reactivity of mixed-metal oxides (51,54,57). The behavior of the $Cr_xMg_{1-x}O$ system is particularly interesting, since it has a much higher DeSOx activity than pure MgO or Cr_2O_3 and illustrates how an element (Cr) present in a mixed-metal oxide can have special chemical properties (51,58).

Figure 11 displays S 2p spectra recorded after adsorbing SO_2 on $Cr_2O_3(0001)$ and $Cr_{0.08}Mg_{0.92}O(100)$ surfaces at 100 K. Not shown are the corresponding results for adsorption of the molecule on a MgO(100) surface (18), which indicate only the presence of SO_3 and SO_4 as seen in Figure 3 for SO_2 adsorption at 300 K. Upon the dosing of 1 langmuir of SO_2 to $Cr_2O_3(0001)$, one sees a set of three doublets which point out the presence of SO_4, SO_3 and SO_2 (51). The SO_3 and SO_4 groups probably result from direct reaction of SO_2 with oxygen sites of the surface:

$$SO_2(\text{gas or ads}) + nO(\text{surf}) \rightarrow SO_{2+n}(\text{ads})\ n = 1,2 \quad [2]$$

After heating the $SO_2/Cr_2O_3(0001)$ system from 100 to 350 K, one sees the disappearance of the signals for SO_3 and SO_2, while the features for SO_4 clearly grow in intensity. As the temperature of the sample is raised, the O atoms of the oxide gain mobility and the formation of SO_4 according to reaction [2] or a

$$SO_3(\text{ads}) + O(\text{surf}) \rightarrow SO_4(\text{ads}) \quad [3]$$

transformation is easier. The metal centers of Cr_2O_3(0001) are able to adsorb SO_2 at low temperatures, but upon heating the molecule does not dissociate on the surface. In this respect, the Cr_2O_3(0001) surface shows a reactivity similar to that of MgO(100).

Photoemission results for the adsorption of SO_2 on a $Cr_{0.08}Mg_{0.92}O$(100) surface at 100 K are shown in the right-side panel of Figure 11 (51). A very small dose of 0.05 langmuir produces mainly peaks for adsorbed SO_2. Since these features are not seen on MgO(100), they can be assigned to SO_2 bonded to Cr atoms. They do not grow much with further exposure to SO_2 because the amount of Cr atoms in the oxide surface is small (51). A 1 langmuir dose of SO_2 leads to a spectrum dominated by the signal for SO_3 species. After depositing a SO_2 multilayer and heating to 150 K, the S 2p spectrum is characterized by intense signals for SO_4 and SO_3, but features appear at ~ 161 eV due to Cr-bonded S adatoms (51). These features grow when the sample temperature is raised from 150 to 450 K. At the same time, there is an increase in the SO_4 signal, and the signals for SO_3 and SO_2 decrease. The reaction that deposits S atoms on the surface

$$SO_n(ads) \rightarrow S(ads) + nO(ads) \quad [4]$$

also frees O atoms that can be used to transform SO_3 into SO_4. The results in Figure 11 indicate that a $Cr_{0.08}Mg_{0.92}O$(100) surface is much more active for the dissociation of S-O bonds than Cr_2O_3(0001) or MgO(100). An identical conclusion can be reached after comparing XANES results for the adsorption of SO_2 on a $Cr_{0.06}Mg_{0.94}O$ catalyst and pure powders of Cr_2O_3 or MgO (51).

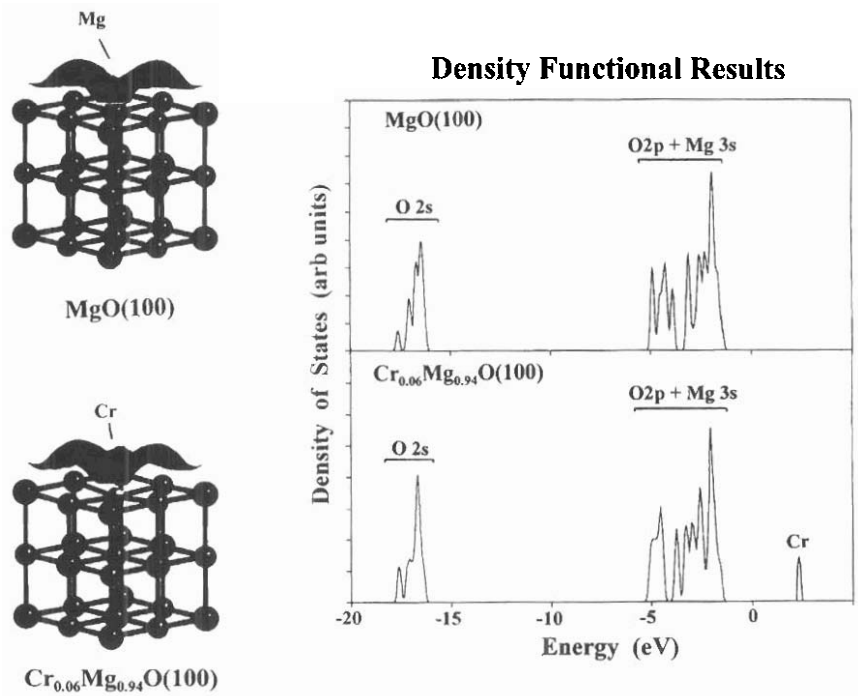

Figure 12. The side of the figure displays calculated electron-density plots for MgO(100), top, and $Cr_{0.06}Mg_{0.94}O$(100), bottom, surfaces. For simplicity, only a few metal and oxygen atoms of each system are shown. The graph in the right-side of the figure shows the calculated DOS for the occupied bands of the MgO(100) and $Cr_{0.06}Mg_{0.94}O$(100) systems (51).

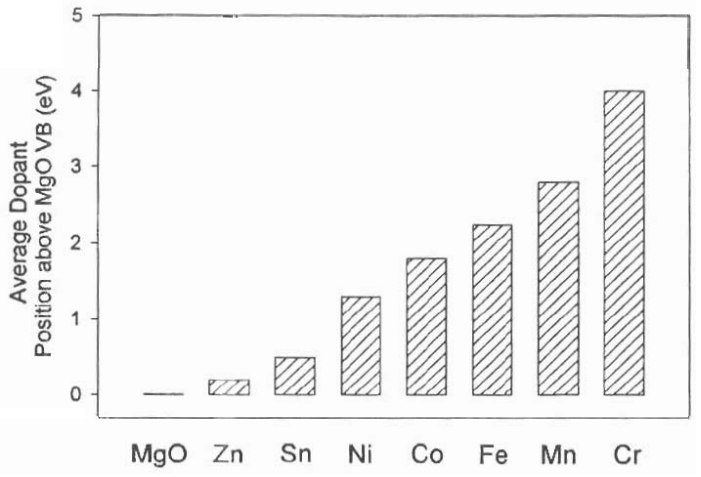

Figure 13. Calculated average position for the dopant levels in $TM_{0.06}Mg_{0.94}O(100)$ surfaces (TM= Zn, Sn, Ni, Co, Fe, Mn or Cr). The values reported are with respect to the top of the MgO valence band (59).

Density-functional slab calculations were used to study the interaction of SO_2 with a $Cr_{0.06}Mg_{0.94}O(100)$ surface (51). Figure 12 shows plots for the electron density around Mg and Cr surface atoms in MgO(100) and $Cr_{0.06}Mg_{0.94}O(100)$. In the case of MgO(100), the total electron density on the Mg atoms is small (20,21,51), and the electron density plot is characterized by maxima located on top of the oxygen atoms. On the other hand, for $Cr_{0.06}Mg_{0.94}O(100)$, one finds a substantial electron density around the Cr atoms. Figure 12 also displays calculated density-of-states (DOS) plots for MgO(100) and $Cr_{0.06}Mg_{0.94}O(100)$. These graphs include only occupied states. In the mixed-metal oxide, the occupied Cr 3d states are less stable energetically than the levels in the occupied (O 2p + Mg 3s) bands of MgO. This theoretical prediction has been corroborated by valence photoemission spectra (54). Thus, from an electronic viewpoint, the Cr centers in a $Cr_{0.06}Mg_{0.94}O(100)$ surface are very well suited for interactions with the LUMO of SO_2 (51). For the adsorption sites of $Cr_{0.06}Mg_{0.94}O(100)$, density-functional calculations give SO_2 adsorption energies 10-20 kcal/mol larger than those on adsorption sites of MgO(100). Even more important, upon adsorption of SO_2 on $Cr_{0.06}Mg_{0.94}O(100)$, the S-O distances increase from 1.43 Å to ~ 1.54 Å making easier the decomposition of the molecule (51).

Spectra of Cr core-level photoemission and Cr L-edge XANES indicate that the formal oxidation state of the chromium atoms in $Cr_{0.06}Mg_{0.94}O$ is closer to "+2" than to "+3" as found in Cr_2O_3 (51,58). Cr^{2+} can be expected from a charge balance in a $Cr_xMg_{1-x}O$ solid solution if one assumes formal charges of "-2" and "+2" for O and Mg, respectively. The key to the special chemical activity of $Cr_{0.06}Mg_{0.94}O$ is in the electronic properties of chromium: the dopant agent is not fully oxidized (i.e., not in a high oxidation state) and provides occupied electronic levels with a low stability (51, 54).

In addition to chromium, other metals can be used when doping MgO (51, 54, 58, 59). The results of density-functional calculations indicate that occupied states with a low stability also can be obtained after doping magnesium oxide with Co, Fe, or Mn. Figure 13 displays the calculated

relative position of the dopant levels in a series of $TM_{0.06}Mg_{0.94}O(100)$ systems (TM= Zn, Sn, Ni, Co, Fe, Mn, or Cr). In these mixed-metal oxides, the instability of the TM 3d band increases as one moves from right to left in the 3d series. The effects of an early transition metal on the electronic properties of MgO are stronger than those of s,p metals such as Zn or Sn. The predicted trends agree well with results of valence photoemission for $Zn_{0.06}Mg_{0.94}O$, $Ni_{0.06}Mg_{0.94}O$, $Fe_{0.05}Mg_{0.95}O$ and $Cr_{0.07}Mg_{0.93}O$ (24,54,59). XANES and photoemission experiments reveal that the position of the dopant-induced levels is critical for DeSOx reactions on $TM_xMg_{1-x}O$ (24,51,54). Thus, $Cr_{0.07}Mg_{0.93}O(100)$ and $Fe_{0.05}Mg_{0.95}O(100)$ are able to fully dissociate SO_2 upon adsorption at 300 K, whereas $Zn_{0.06}Mg_{0.94}O(100)$ and $Sn_{0.07}Mg_{0.93}O(100)$ just adsorb the molecule to form SO_3/SO_4.

6. Conclusions

On pure stoichiometric oxides (MgO, Al_2O_3, TiO_2, Cr_2O_3, Fe_2O_3, NiO, CuO, ZnO, ZrO_2, V_2O_5, MoO_3, $CoMoO_4$ and $NiMoO_4$), SO_2 reacts with the O centers to form SO_3 or SO_4 species that decompose at elevated temperatures. Adsorption on the metal cations occurs below 300 K and does not lead to cleavage of S-O bonds. In typical oxides, the occupied cation bands are too stable for effective bonding interactions with the LUMO of SO_2. *To activate an oxide for S-O bond cleavage, one has to generate occupied metal states above the valence band of the oxide.* This basic requirement can be accomplished by the creation of O vacancies, alkali promotion, or doping with a transition metal.

Acknowledgements

Many of the studies described in this review were done in collaboration with S. Chaturvedi, A. Freitag, L. González, J. Hrbek, T. Jirsak, M. Kuhn, J.Z. Larese, A. Maiti, and M. Pérez. Many thanks to all of them for their valuable contributions. The author is grateful to J. Evans and H. Lee for several interesting conversations on DeSOx chemistry. The research carried out at Brookhaven National Laboratory was supported by the US Department of Energy (Divisions of Chemical and Materials Science) under contract DE-AC02-98CH10086.

References

1. ADLKOFER J. ***Handbook of Heterogeneous Catalysis***; Ertl, G., Knözinger, H., WEITKAMP J. Volume 4 Wiley-VCH, New York (USA), 1776, 1997.
2. STERN A.C., BOUBEL R.W., TURNER D.B., Fox D.L. ***Fundamentals of Air Pollution***, 2nd ed, Academic Press: Orlando, FL (U.S.A), 1984.
3. PIÉPLU A., SAUR O., LAVALLEY J.C., LEGENDRE O., NÉDEZ C. ***Catal Rev -Sci Eng*** 40: 409, 1998.
4. ARMOR J.N. ***Environmental Catalysis***, ACS Symposium Series No 552 American Chemical Society: Washington DC (USA), 1994.
5. SHELEF M., MCCABE R.W. ***Catal Today*** 62: 35, 2000.
6. BARTHOLOMEW C.H., AGRAWAL P.K., KATZER J.R. ***Adv Catal*** 31: 135, 1982.
7. RODRIGUEZ J.A., HRBEK J. ***Accounts of Chemical Research*** 32: 719, 1999.
8. BECK D.D., SOMMERS J.W., DIMAGGIO C.L. ***Appl Catal B*** 11: 273, 1997.
9. BECK D.D. ***Catalyst Deactivation*** 111: 21, 1997.
10. GORTE R. private communication.
11. SLACK A.V., HOLLIDEN G.A. ***Sulfur Dioxide Removal from Waste Gases*** 2nd Edition Noyes Data Corporation: Park Ridge, NJ (USA), 1975.
12. CENTI G., PASSARINI N., PERATHONER S., RIVA A. ***Ind Eng Chem Research*** 1:1947, 1992.

13. WAQIF M., SAUR O., LAVALLEY J.C., PERATHONER S., CENTI G. ***J Phys Chem*** 95: 4051, 1991.
14. ZHU T., KUNDAKOVIC K., DREHER A., FLYTZANI-STEPHANOPOULOS M. ***Catal Today*** 50: 381, 1999.
15. LIU W., WADIA C., FLYTZANI-STEPHANOPOULOS M. ***Catal Today*** 28: 391, 1996.
16. RODRIGUEZ J.A., JIRSAK T., CHATURVEDI S., KUHN M. ***Surf Sci*** 442: 400, 1999.
17. RODRIGUEZ J.A., JIRSAK T., CHATURVEDI S., DVORAK J. ***J Molecular Catalysis A*** 167: 47, 2001.
18. RODRIGUEZ J.A., PÉREZ M., JIRSAK T., GONZÁLEZ L., MAITI M. ***Surf Sci*** 477: L279, 2001.
19. RODRIGUEZ J.A., JIRSAK T., FREITAG A., LARESE J.Z., MAITI A. ***J Phys Chem B*** 104: 7439, 2000.
20. PACCHIONI G., CLOTET A., RICART J.M. ***Surf Sci*** 315: 337, 1994.
21. SCHNEIDER W.F., LI J., HASS K.C. ***J Phys Chem B*** submitted.
22. WAQIF M., SAAD A.M., BENSITEL M., BACHELIER J., SAUR O., LAVALLEY J.C. ***J Chem Soc Faraday Trans*** 88: 2931, 1992.
23. RODRIGUEZ J.A., JIRSAK T., FREITAG A., HANSON J.C., LARESE J.Z., CHATURVEDI S. ***Catal Lett*** 62: 113, 1999.
24. RODRIGUEZ J.A., JIRSAK T., GONZÁLEZ L., EVANS J., PERÉZ M., MAITI A. To be published.
25. RODRIGUEZ J.A., HANSON J.C., CHATURVEDI S., BRITO J.L. ***Studies in Surf Sci Catal*** 130: 2795, 2000.
26. WARBURTON D.R., PUNDIE D., MURYN C.A., PRAHAKARAN K., WINCOTT P.L., THORTON G. ***Surf Sci*** 269/270: 305, 1992.
27. MURYN C., PURDIE D., HARDMAN P., JOHNSON A.L., PRAKASH N.S., RAIKER G.N., THORTON G., LAW, D. ***Faraday Discuss Chem Soc*** 89: 77, 1990.
28. KURTZ R.L., HENRICH V.E. ***Phys Rev B*** 36: 3413, 1987.
29. ZHANG Z., HENRICH V.E. ***Surf Sci*** 225: 47,1990.
30. LI X., HENRICH V.E. ***Phys Rev B*** 48: 17486, 1993.
31. CHATURVEDI S., RODRIGUEZ J.A., JIRSAK T., HRBEK J. ***J Phys Chem B*** 102: 7033, 1998.
32. JIRSAK T., RODRIGUEZ J.A., HRBEK J. ***Surf Sci*** 426: 319, 1999.
33. PACCHIONI G., RICART J.M., ILLAS F. ***J Am Chem Soc*** 116: 10152, 1994.
34. RODRIGUEZ J.A., JIRSAK T., HRBEK J. ***J Phys Chem B*** 103: 1966, 1999.
35. RODRIGUEZ J.A., CHATURVEDI S., KUHN M., HRBEK J. ***J Phys Chem B*** 102: 5511, 1998.
36. MULLINS D.R., OVERBURY S.H., HUNTLEY D.R. ***Surf Sci*** 409: 307, 1998.
37. LIU G., RODRIGUEZ J.A., HRBEK J., DVORAK J., PEDEN C.H.F. ***J Phys Chem B*** in press, 2001.
38. TSCHOPE A., LIU W., FLYTZANI-STEPHANOPOULOS M., YING J.Y. ***J Catal*** 157: 42, 1995.
39. KOLMAKOV A., STULZ J., GOODMAN D.W. ***J Chem Phys*** 113: 7564, 2000.
40. DE CAROLIS S., PASCUAL J.L., PETTERSON L.G.M., BAUDIN M., WOJCIK M., HERMANSSON K., PALMQVIST A.E.C., MUHAMMED M. ***J Phys Chem B*** 103: 7627, 1999.
41. MITCHELL M.B., SHEINKER V.K., WHITE M.G. ***J Phys Chem*** 100: 7550, 1996.
42. DEO A.V., DALLA LANA I.G., HABGOOD H.W. ***J Catal*** 21: 270, 1971.
43. CHUNG J.S., PAIK S.C., KIM H.S., LEE D.S., NAM I.S. ***Catal Today*** 35: 37, 1997.
44. CAMPBELL C.T. ***Surf Sci Reports*** 27:1, 1997.
45. RODRIGUEZ J.A., JIRSAK T., CHATURVEDI S., HRBEK J. ***Surf Sci*** 407: 171, 1998.

46. JIRSAK T., DVORAK J., RODRIGUEZ J.A. ***J Phys Chem B*** 103: 5550, 1999.

47. LEYSEN R., HOPKINS B.J., TAYLOR P.A. ***J Phys C: Solid State Physics*** 8: 907, 1975.

48. TAYLOR P.A., HOPKINS B.J. ***J Phys C: Solid State Physics*** 11: L643, 1978.

49. SNYDER J.A., JAFFE J.E., LIN Z., HESS A.C., GUTOWSKI M. ***Surf Sci*** 445: 495, 2000.

50. BREDOW T., APRÁ E., CATTI M., PACCHIONI G. ***Surf Sci*** 418:150, 1998.

51. RODRIGUEZ J.A., JIRSAK T., PÉREZ M., CHATURVEDI S., KUHN M., GONZALEZ L., MAITI A. ***J Am Chem Soc*** 122:12362, 2000.

52. RODRIGUEZ N.M., SOLED S.L., HRBEK J. ***Mater Research Soc Symp Proc*** 497, 1997.

53. ***Symposium on the Characterization of Mixed-Metal Oxide Catalysts; 215th National Meeting of the American Chemical Society,*** Dallas, TX American Chemical Society, Washington DC (USA), 1998.

54. RODRIGUEZ J.A., JIRSAK T., PÉREZ M., GONZÁLEZ L., MAITI A. ***J Chem Phys*** 114: 4186, 2001.

55. HENRICH V.E., COX P.A. ***The Surface Science of Metal Oxides***, Cambridge University Press, Cambridge (U.K.), 1994.

56. MAMONTOV E., EGAMI T., BREZNY R., KORANNE M., TYAGI S. ***J Phys Chem B*** 104: 11110, 2000.

57. RODRIGUEZ J.A., HANSON J.C., CHATURVEDI S., MAITI A., BRITO J.L. ***J Phys Chem B*** 104: 8145, 2000.

58. FISHER I., ZHANG L., WU Y., EVANS J., LEE H. Private Communication.

59. RODRIGUEZ J.A., PÉREZ M., JIRSAK T., GONZÁLEZ L., MAITI A. LARESE J.Z. ***J Phys Chem B*** 105: 5497, 2001.